ChemComm

Mechanism of Hydrogen Storage on Fe3B

Journal:	*ChemComm*
Manuscript ID	CC-COM-05-2020-003741.R3
Article Type:	Communication

COMMUNICATION

Mechanism of Hydrogen Storage on Fe_3B

Zhao Ding [a,c], Hao Li [d], Ge Yan [b], Weijie Yang *[b], Zhengyang Gao [b], Wenhui Ma [e] and Leon Shaw [c]

Received 00th January 20xx,
Accepted 00th January 20xx

DOI: 10.1039/x0xx00000x

Recent experimental finding has indicated that Fe_3B has the capacity to absorb and release hydrogen. However, the mechanism has not been clarified. Here, for the first time, the characteristics were investigated through the electronic structures and energies of H_2 molecules adsorbed on Fe_3B using density functional theory calculations. Most importantly, this work provides a guideline for experimental investigation on wide-source and low-cost Fe-based hydrogen storage materials.

The growing awareness of environmental pollution caused by the burning of conventional fossil fuel has motivated a large number of studies on renewable hydrogen fuel source. Meanwhile, plenty of studies have focused on the discovery and synthesis of solid-state materials for onboard hydrogen storage, due to its advantages of moderate pressure, light container, and flexible shape, compared to the compressed gaseous and cryogenic liquid hydrogen technologies.[1, 2] However, no material so far can meet the expectations of industrial standards of on-board hydrogen storage systems (which releases and uptakes 7.5 wt. % H_2 at the temperature of 95~105 ℃).[3, 4]

Lately, our group has devised a novel process with high-energy ball milling (BM) of MgH_2 at ambient temperature in conjunction with aerosol spraying (AS) of $LiBH_4$ dissolved in tetrahydrofuran (THF) solution.[5-10] Through the BMAS process, we have shown that the reversible hydrogen storage capacity of $LiBH_4$ + MgH_2 mixture can achieve as high as ~4.11 wt.% in the solid state without any catalyst, and $Mg(BH_4)_2$ has been formed via the direct reaction between MgH_2 and $LiBH_4$ for the first time as expressed in Reaction (1). [5, 7] Fe comes from the wear of stainless steel balls during ball milling, would react with B that comes from the gradual decomposition of $Mg(BH_4)_2$ via reaction (2), to form Fe_3B, as shown in reaction (3). The formation of Fe_3B has been ascribed to the interesting phenomenon that the amount of hydrogen uptake in hydrogenation is higher than the hydrogen released in the previous dehydrogenation (starting from the second cycle). [5] The hydrogen amount of desorption and absorption as a function of dehydrogenation and re-hydrogenation cycles was plotted in a histogram in Figure S1.

$$2\,LiBH_4\,(s) + MgH_2\,(s) = Mg(BH_4)_2(s) + 2\,LiH\,(s) \quad (1)$$

$$Mg(BH_4)_2\,(s) \rightarrow MgH_2\,(s) + 2\,B\,(s) + 3\,H_2\,(g) \quad (2)$$

$$3\,Fe\,(s) + B\,(s) = Fe_3B\,(s) \quad (3)$$

Noted the self- and acroscopic diffusion of the hydrogen atom in amorphous Fe_3B have been studied with first-principles calculations.[11, 12] However, to the best of our knowledge, there is currently no report of the interaction between Fe_3B and H_2 for hydrogen storage. Xie and Gu[13] reported that H_2 could dissociate and interact with iron on Fe(110), forming stable Fe-H bonds. Pozzo and Alfè[14] have further confirmed that theoretically, doping a Fe on Mg(0001) surface results in facile H_2 dissociation at the Fe site, due to the very low dissociation barrier. Besides, many studies[15-20] have shown that hydrides can be formed easily on Fe-related sites, so it is not groundless to consider Fe-related materials such as Fe_3B as a new type of hydrogen storage material.

In this study, for the first time, the mechanism of H_2 adsorption and desorption on Fe_3B was investigated using density functional theory (DFT) calculations. Firstly, geometric structures of Fe_3B model and adsorption characteristics of H_2 on Fe_3B were studied through the analysis of adsorption configurations and adsorption energies. Secondly, the adsorption mechanism of H_2 on Fe_3B was investigated through the calculated electron density difference (EDD), projected density of states (PDOS), and electron localization function (ELF). Finally, thermodynamic analysis and *ab initio* molecular dynamics (AIMD) simulations, were adopted to study the dehydrogenation characteristic of Fe_3B. This work provides an understanding of the hydrogenation and dehydrogenation over the Fe_3B surface, so as to design similar Fe-based compounds as a viable system for reversible hydrogen storage applications near ambient temperature.

The Fe_3B structures were modelled in the form of orthorhombic crystal, consisting of 24 Fe and 8 B atoms, with the lattice parameters of a=9.70, b=7.01, and c=4.23. Fig. 1 shows the stereogram of the stable crystal structure. To understand the binding mechanism between Fe and B, the PDOS of Fe_3B was calculated (Fig. 1). The *d* orbital of Fe is asymmetric with the two spin states, which indicates

[a] *The State Key Laboratory of Refractories and Metallurgy, Institute of Advanced Materials and Nanotechnology, Wuhan University of Science and Technology, Wuhan, China*
[b] *School of Energy, Power and Mechanical Engineering, North China Electric Power University, Baoding, China*
[c] *Department of Mechanical, Materials and Aerospace Engineering, Illinois Institute of Technology, Chicago, Illinois, USA*
[d] *Department of Physics, Technical University of Denmark, 2800 Kongens Lyngby, Denmark*
[e] *Faculty of Metallurgical and Energy Engineering, Kunming University of Science and Technology, Kunming, China*
* Corresponding Author: yangwj@ncepu.edu.cn
Electronic Supplementary Information (ESI) available: See DOI: 10.1039/x0xx00000x

that the system is magnetic. The calculated average magnetic moment of Fe_3B is 1.70 μB, which is significantly larger than that of FeB (1.13 μB).[21] Furthermore, the *d* orbital of Fe hybridizes with the *p* orbital of B mainly in the energy range from -3 to 3 eV. Such a phenomenon is consistent with the work of Zhang et al.[22] These hybridizations play important roles to form a strong Fe-B bond, leading to a rational Fe_3B system that is sufficiently stable to achieve the process of H_2 adsorption.

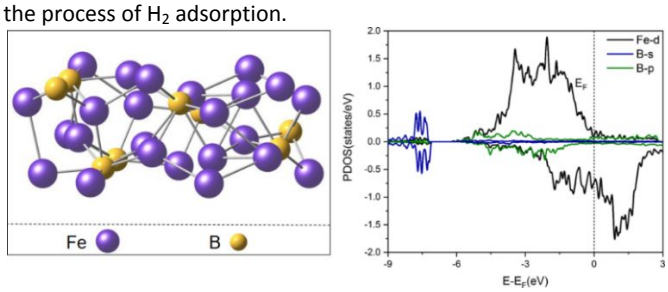

Fig. 1 Optimized geometric structure and PDOS plot of Fe_3B.

Based on the modelled Fe_3B structure, potential adsorption sites and different orientations of H_2 were calculated to obtain the most stable adsorption configurations, as shown in Fig. 2. The corresponding adsorption energy, charge variation, and bond length are listed in Table S1.

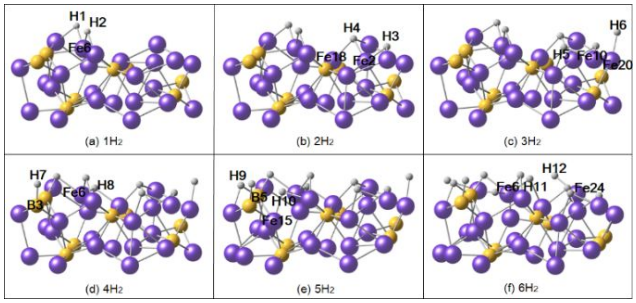

Fig. 2 Optimized geometric structures of nH_2 (*n*=1-6) adsorbed on Fe_3B. Purple, orange, and gray spheres represent Fe, B, and H atoms, respectively.

As shown in Fig. 2a, the first H_2 is adsorbed on the Fe site, with the adsorption energy of -1.00 eV. Such strong chemisorption is accompanied by the dissociation of H_2, with the H-H elongating to 2.49 Å compared to that of 0.75 Å in the H_2 gas molecule. The distances between H and the nearest Fe are 1.68 and 1.67 Å. Fig. 2b explores possible adsorption sites on the basis of Fig. 2a, obtaining the stable configuration of the second H_2 adsorption on Fe_3B. The adsorption energy is -1.17 eV with an extinct increase. It should be noted that this H_2 dissociates greater than the first H_2. Similarly, the configurations of Fe_3B with the adsorption of the third to sixth H_2 molecules were also optimized (Fig. 2c-2f). There is an increasing trend of adsorption energy from the first H_2 to the third H_2 where H_2 molecules are both adsorbed on the Fe sites. Fig. 2c shows the maximum adsorption energy of -1.19 eV with the hydrogen coverage of 0.5 on Fe_3B. In terms of the fourth and fifth H_2, H started to be adsorbed on the B sites rather than Fe sites. Meanwhile, the adsorption energy decreases from the adsorption of the fourth H_2 to the sixth H_2. It should be noted that, the six H_2 molecules are all absorbed on the five Fe atoms on the top layer as shown in Fig. 2, which indicates a corresponding hydrogen storage capacity of 4.15 wt.% at the surface. Though the adsorption energies in these three models are relatively weak, H_2 molecules all dissociate in the whole six adsorption models. In comparison, Liu et al. [23] studied six H_2 adsorptions on Ti-decorated B38 fullerene with the maximum adsorption energies of 0.45eV, which shows much inferior H_2 adsorption ability than that of Fe_3B investigated in this work.

Then, we performed further research to compare the hydrogenation capacity between the defective and perfect models of the 1H2 system. Fe6 vacancy and its nearest two vacancies (Fe8 vacancy and Fe22 vacancy) were studied(Fig. S2). Our results showed that the absorption energy of Fe6 vacancy structure in Fig. S2 (a) and Fe8 vacancy structure in Fig. S2 (b) are -1.00 and -1.02 eV, respectively, being similar to that of perfect model (-1.00 eV). The Fe22 vacancy structure in Fig. S2(c) has the value of -0.32 eV, much smaller than that of perfect model. Charge changes of the adsorption sites in the perfect and defective models were further investigated, as shown in Table S2. In the model with Fe6 vacancy, B5 has more negative charge changes, indicating more facile hydrogen desorption. In the model with Fe8 vacancy, Fe6 loses most of the charges. However, the model with Fe22 vacancy has weak hydrogen adsorption capacity with small H-H elongation. Fe6 obtained 0.12 e, resulting in weak adsorption capacity. In conclusion, it is expected that the defect sites of Fe_3B have less significant improvement in hydrogen absorption.

To further understand the adsorption properties of H_2 onto Fe_3B, the relevant charge, electronic, and bonding properties are analyzed by EDD, PDOS, and ELF.

EDD is used as a subtle tool to highlight the bonding mechanism in the process of adsorption. The Bader charge changes of the first to sixth H_2 molecules and substrates are summarized in Table S1, revealing that H_2 always gains electrons from the substrates during hydrogen adsorption. With smaller energies, the adsorption systems of the fifth and sixth H_2 would have less electron transfer. The specific charge changes of all the hydrogen atoms and adsorption sites in the current hydrogenation process are listed in Table S3. According to the specific charge analysis (Table S3), the obvious charge variation difference between Fe and H can show the formation trend of stable ionic bonds which leads to large adsorption energies. Considering the similar charge variation between B and H, there seem to be covalent bonds. To further analyze the charge properties of the first to six H_2 molecules adsorption on Fe_3B, EDD maps at the top and side view are plotted in Fig. 3. Fe, B, and H atoms are colored in purple, orange, and gray, respectively.

Fig. 3 shows that H_2 is always surrounded by yellow regions, which indicates that there are aggregations of electrons. Fe and B are always surrounded by cyan regions especially at the adsorption site, and lower-level atoms have almost no electronic gain or loss. Fig. 3 further confirms that some charges have transferred from the Fe or B atoms to H which is consistent with our Bader charge analysis. Moreover, the first H_2 has the largest change in the electrons gain mainly in (d)-(f). The adsorption site of the fourth and sixth H_2 is Fe6 which is also the adsorption site of the first H_2, leading the first H_2 to reduce electrons. The obvious reduction in the adsorption energy from the third to the fourth H_2 can be attributed to the following two possibilities. The first reason is that it turns out to be very difficult to transfer electrons from B to H because B possesses weaker metallicity than Fe. The second reason is that Fe6 has already been

occupied by H8, which makes it too saturated to transfer more electrons.

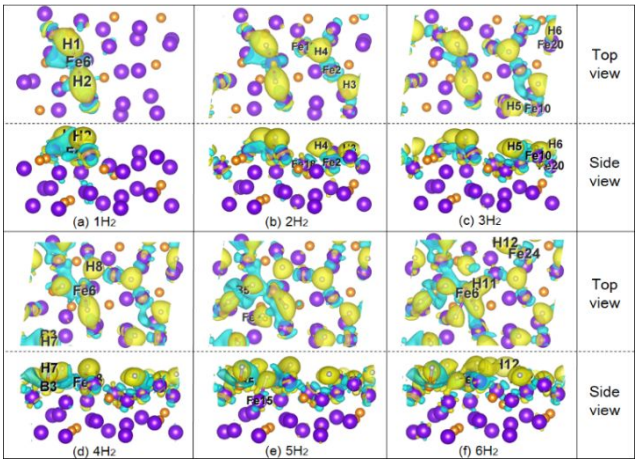

Fig. 3 EDD maps of the first to sixth H_2 adsorbed on Fe_3B. Cyan and yellow regions represent electron loss and gain, respectively.

To further analyze the effect of Fe_3B surface on H_2 adsorption, the PDOS profiles of the first to sixth H_2 on Fe_3B are plotted in Fig. S3. It can be seen that the 3*d* orbitals of Fe contribute significantly when the binding is between Fe and H. When it is between B and H, the *s* and *p* orbitals contribute to different energy ranges. Therefore, the Fe-*d*, B-*s*, and B-*p* orbitals before and after adsorption are all studied. The *s* orbitals of H in adsorbed and gas states are plotted in red line and pink solid fill, respectively. The *d* orbitals of Fe or *s* orbitals of B are both plotted in black and blue lines before and after adsorption. Besides, the *p* orbitals of B are plotted in purple and green lines before and after adsorption. The dotted line in the figure is to show the change of energy width of the orbit. We choose the most representative interaction atoms including Fe6-H2, Fe18-H4, Fe20-H6, B3-H7, B5-H9, and F66-H11. After adsorption, there is a bonding between Fe and H. The *s* states of H shift down to lower energy states, which are further away from the Fermi level. From Fig. S3a-c, H-*s* orbitals keep moving to lower states and then move to higher states according to Fig. S3d-f. This is consistent with the above-mentioned statement that the adsorption energy climbs up through adsorbing the first to the third H_2 and then decline through adsorbing the fourth to the sixth H_2. Therefore, it is deduced that Fe_3B phase tends to be saturated and not so easy to adsorb H_2 after the adsorption of three H_2. According to the PDOS, Fe-3*d* hybridize with the H-*s* orbitals mainly in the range from -8 to -4 eV. There is a significant increase in the orbital width of Fe atoms and this trend becomes more obvious in Fig. S3a-c. Combining with the evidence that B starts to participate in the fourth and fifth H_2 adsorption systems, it is reasonable to believe that hydrogen is only weakly adsorbed at the B sites. The orbitals of B hybridize with that of H, which is not consistent with the small adsorption energies. However, the charge transfers are relatively small and it may be confirmed that hydrogen adsorption is dominated by charge transfer. The obvious hybrid peak appears between the H-*s* orbital and the B-*s* or B-*p* orbital. This orbital hybridization tends to form a covalent bond between H and B.

ELF is used to study different bonding interactions. ELF values are calculated from excess kinetic energy density due to the Pauli mutual exclusion and the Thomas–Fermi kinetic energy functional.[24] It should be noted that a higher value of ELF stands for a stronger localization region which is better for finding an electron or a pair of localized electrons. For a covalent bonding, ELF goes to a large value ranging from 0.6 to 1. While for an ionic boning, ELF goes to a small value ranging from 0 to 0.5. The ELF contour maps of the first to sixth H_2 adsorbed on Fe_3B are shown in Fig. 4. Both of the two-dimensional images were calculated from the best plane containing the relevant H_2 and adsorption site. The region with strong localization tends to be red while that with strong delocalization tends to be blue.

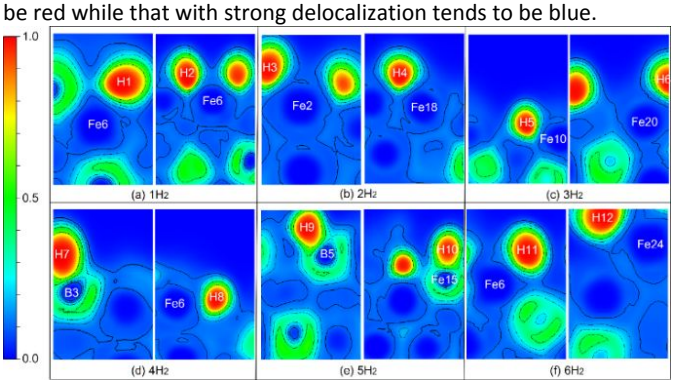

Fig. 4 ELF maps of the first to sixth H_2 adsorbed on Fe_3B.

According to the ELF maps (Fig. 4), the ELF value is close to 1 at the H site, indicating a highly localized electron position. The hydrogen in the gas phase is connected by a highly localized covalent bond, and the degree of electron localization is significantly reduced after full activation. In contrast, the Fe and B sites are highly delocalized since their ELF values are close to zero. These notable differences confirm that Fe_3B donates electrons to H_2. H and Fe/B tend to form ionic bonds because of the relatively low ELF value (0-0.5). The ELF contours of H atoms in (a)-(c) are not spherically shaped but polarized to Fe atoms because of the repulsive force between the negatively charged H atoms. This polarization, in turn, reduces the interaction of H_2 thus leading to a shorter H-H bond. The degree of delocalization degree of B3 and Fe15 atoms in Fig. 4d and 5e are relatively stronger than before, indicating a weak interaction between H_2 and Fe_3B. Therefore, there is a significant decrease in adsorption energies. The smaller increase of adsorption energy finally can be attributed to the reduced delocalization degree of Fe (Fig. 4f).

Firstly, as one of the most important parameters of experiments, the effect of temperature on hydrogen storage should be considered.[25,26] Thermodynamics analysis of the system was conducted for further applications based on the calculation of Gibbs free adsorption energy (ΔG) under different temperatures. The vibrational frequency was performed through the numerical Hessian calculations with finite displacements of ± 0.02Å. In order to evaluate the hydrogen storage capacity, ΔG of the first to the sixth H_2 adsorption on Fe_3B were plotted ranging from 298.15 to 1000 K (Fig. S5). Noted a negative value of ΔG indicates that the adsorption process can occur spontaneously. And the more negative of ΔG, the stronger interaction between H_2 and Fe_3B.

It is found that all of the ΔG values increase with the rise of temperature, indicating that temperature has an inhibition effect on the adsorption. From Fig. S4, it is worth noting that the adsorption order is consistent with the above calculations and analysis. All of the ΔG values of the first, second, and third H_2 adsorption remain

negative under a lower temperature range. In contrast, the ΔG values of the fourth, fifth, and sixth H_2 adsorption are mostly positive which indicates that H_2 adsorption is no longer easy to occur at Fe_3B. As expected, the absorption of the third H_2 is the most favorable reaction under 500 K. Meanwhile, according to Fig. S4, for the required condition for the release of the first, second, third, fourth, fifth, and sixth H_2 are all under the experimental temperature (538 K).

In order to further investigate the dehydriding ability and thermal stability of Fe_3B, desorption kinetics of the adsorbed H_2 on Fe_3B+6H_2 were investigated by AIMD. The AIMD simulations was performed using the VASP package, for up to 10 ps with a time step of 1 fs. To be consistent with the experimental conditions, the whole simulation process was also conducted under 538 K. The displacement of hydrogen was measured as the bond length of Fe-H and marked in blue in Fig. 5. As shown, H begins to displace after about 5500 fs of simulation. The peak occurs at about 6000 fs, which means the longest displacement with a value of 15.98 Å. According to Fig. 5, the potential energy of Fe_3B+6H_2 (black line), is constantly decreasing until 6000 steps, where shows an equilibrium state shock. The escaped H in Fig. 5 are H1 and H12. They both have smaller charge transfers in adsorption processes, so they interact with Fe_3B weakly and are easy to be removed. With the AIMD simulation results, it can be concluded that Fe_3B has the ability to release H_2 at 538 K, in good agreement with previous experiments.[5] Since Fe is one of the most abundant elements in the Earth's crust, both the origin and cost of Fe-based materials are rather competitive for hydrogen storage when compared to Mg-based materials.

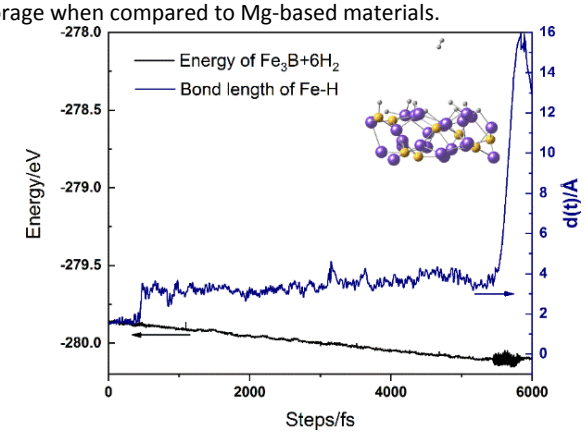

Fig. 5 AIMD profiles of the H_2 desorption on Fe_3B+6H_2 at 538 K.

In this paper, the adsorption characteristics of the first to sixth H_2 on Fe_3B were studied by DFT calculations. Dissociative adsorption is a favorable adsorption type of H_2, resulting in two separate H on Fe_3B. The adsorption energy increases at first and then decreases with a higher H coverage, reaching saturation when the H_2 coverage is 0.5. The Fe sites are more favorable for hydrogen activation and adsorption, compared to the B sites. The interaction type of H_2 on Fe_3B is dominated by ionic bonds which brings about a strong adsorption strength. Dehydrogenation performance of Fe_3B can be ensured under the temperature of 538 K, in good agreement with the previous experiments.

This work was supported under the U.S. National Science Foundation (NSF) with the Award no. CMMI-1261782, Beijing Municipal Natural Science Foundation (2182066), Natural Science Foundation of Hebei Province of China (B2018502067) and Fundamental Research Funds for the Central Universities (JB2015RCY03 and 2017XS121).

Conflicts of interest

There are no conflicts to declare.

References

1. Z. Xiong, C. K. Yong, G. Wu, P. Chen, W. Shaw, A. Karkamkar, T. Autrey, M. O. Jones, S. R. Johnson and P. P. Edwards, *Nat. Mater.* , 2008, **7**, 138.
2. P. Chen, Z. Xiong, J. Luo, J. Lin and K. L. Tan, *Nature*, 2002, **420**, 302.
3. Z. Ding, S. Li, Y. Zhou, Z. Chen, W. Yang, W. Ma and L. Shaw, *Nano Materials Science*, 2020, **2**, 109-119.
4. Target Explanation Document: Onboard Hydrogen Storage for Light-Duty Fuel Cell Vehicles, 2017.
5. Z. Ding, H. Li and L. Shaw, *Chemical Engineering Journal*, 2020, **385**, 123856.
6. Z. Ding, Y. Lu, L. Li and L. Shaw, *Energy Storage Materials*, 2019, **20**, 24-35.
7. Z. Ding and L. Shaw, *ACS Sustainable Chemistry & Engineering*, 2019, **7**, 15064-15072.
8. Z. Ding, P. Wu and L. Shaw, *Journal of Alloys and Compounds*, 2019, **806**, 350-360.
9. Z. Ding, X. Zhao and L. L. Shaw, *Journal of Power Sources*, 2015, **293**, 236-245.
10. Y. Zhong, X. Wan, Z. Ding and L. L. Shaw, *International Journal of Hydrogen Energy*, 2016, **41**, 22104-22117.
11. S. Hao and D. S. Sholl, *J Chem Phys.*, 2009, **130**, 244705.
12. S. Hao, M. Widom and D. S. Sholl, *J. Phys.: Condens. Matter* 2009, **21**, 115402.
13. W. Xie, L. Peng, D. Peng, F. L. Gu and J. Liu, *Appl. Surf. Sci.* , 2014, **296**, 47-52.
14. M. Pozzo and D. Alfe, *Int. J. Hydrogen Energy* 2009, **34**, 1922-1930.
15. Y.-C. Liu, K.-T. Chu, R.-L. Jhang, G.-H. Lee and M.-H. Chiang, *Chem. Commun.* , 2013, **49**, 4743-4745.
16. F. Aubertin, U. Gonser and S. Campbell, *J. Phys. F: Met. Phys.* , 1984, **14**, 2213.
17. J. I. van der Vlugt, T. B. Rauchfuss, C. M. Whaley and S. R. Wilson, *JACS* 2005, **127**, 16012-16013.
18. D. Papaconstantopoulos and A. Switendick, *Journal of the Less Common Metals*, 1982, **88**, 273-281.
19. J. Xu, A. Avellan, H. Li, X. Liu and G. V. Lowry, *Advanced Materials*, 2020, 1906910.
20. Z. Cao, H. Li, X. Xu and J. Xu, *Chemical Engineering Journal*, 2020, 124876.
21. A. Gueddouh, B. Bentria, I., K. Lefkaier, Y. Bourourou, *Bulletin of Materials Science*, 2016, **39**, 1427-1434.
22. W. H. Zhang, Z. Q. Lv, Z. P. Shi, S. H. Sun, Z. H. Wang and W. T. Fu, *Journal of Magnetism and Magnetic Materials*, 2012, **324**, 2271-2276.
23. P. Liu, H. Zhang, X. Cheng and Y. Tang, *International Journal of Hydrogen Energy*, 2016, **41**, 19123-19128.
24. J. Santos, W. Tiznado, R. Contreras and P. Fuentealba, *The Journal of chemical physics*, 2004, **120**, 1670-1673.
25. Z. Ding, Z. Chen, T. Ma, C.-T. Lu, W. Ma and L. Shaw, *Energy Storage Materials*, 2020, **27**, 466-477.
26. H. Li, S. Xu, M. Wang, Z. Chen, F. Ji, K. Cheng, Z. Gao, Z. Ding and W. Yang, J. Mater. Chem. A, 2020, **8**, 17987-17997.

For Table of Contents Use Only

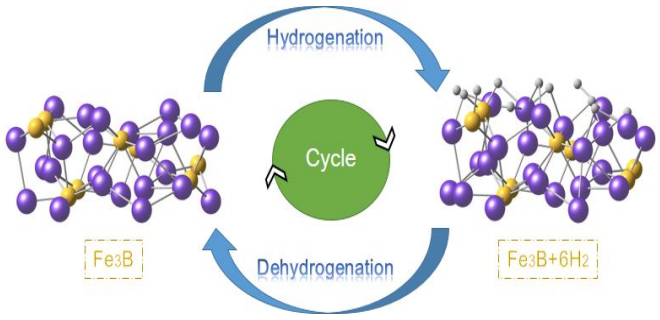

For Fe_3B, the adsorption energy of H_2 reaches the maximum at the coverage of 0.5, and the onset dehydrogenation temperature is 538 K.